Photodissociation transition states characterized by chirped pulse millimeter wave spectroscopy

Kirill Prozument[a,b], Joshua H. Baraban[a,c], P. Bryan Changala[d], G. Barratt Park[a,e,f], Rachel G. Shaver[a], John S. Muenter[g], Stephen J. Klippenstein[b], Vladimir Y. Chernyak[h,i], and Robert W. Field[a,1]

[a]Department of Chemistry, Massachusetts Institute of Technology, Cambridge, MA 02139; [b]Chemical Sciences and Engineering Division, Argonne National Laboratory, Lemont, IL 60439; [c]Department of Chemistry, Ben-Gurion University of the Negev, Beer-Sheva 8410501, Israel; [d]JILA, Department of Physics, University of Colorado, Boulder, CO 80309; [e]Max Planck Institute for Biophysical Chemistry, 37077 Goettingen, Germany; [f]Institute of Physical Chemistry, University of Goettingen, 37077 Goettingen, Germany; [g]Department of Chemistry, University of Rochester, Rochester, NY 14627; [h]Department of Chemistry, Wayne State University, Detroit, MI 48202; and [i]Department of Mathematics, Wayne State University, Detroit, MI 48202

Contributed by Robert W. Field, October 31, 2019 (sent for review July 5, 2019; reviewed by Brooks H. Pate and Richard N. Zare)

The 193-nm photolysis of CH_2CHCN illustrates the capability of chirped-pulse Fourier transform millimeter-wave spectroscopy to characterize transition states. We investigate the HCN, HNC photofragments in highly excited vibrational states using both frequency and intensity information. Measured relative intensities of $J = 1$–0 rotational transition lines yield vibrational-level population distributions (VPD). These VPDs encode the properties of the parent molecule transition state at which the fragment molecule was born. A Poisson distribution formalism, based on the generalized Franck–Condon principle, is proposed as a framework for extracting information about the transition-state structure from the observed VPD. We employ the isotopologue CH_2CDCN to disentangle the unimolecular 3-center DCN elimination mechanism from other pathways to HCN. Our experimental results reveal a previously unknown transition state that we tentatively associate with the HCN eliminated via a secondary, bimolecular reaction.

transition state | photolysis | vibrational population distribution | chirped-pulse millimeter-wave spectroscopy | vibrational satellites

The primary objective of transition-state spectroscopy (1–4) is experimental observation of the most hidden aspect of a chemical reaction: the transition state (TS). Formally, the TS is a hypersurface in phase space that delineates reactants from products. Reactants that pass through this hypersurface in the forward direction proceed on to products, and vice versa. Since molecules are never stabilized on the TS dividing surface, one cannot directly observe the TS. Instead, with TS spectroscopy one aims to observe spectroscopic features of the structures surrounding this TS dividing surface. The 10- to 100-fs (5) duration passage through the neighborhood of the TS determines the reaction rate and molecular product ratios and is also a key determining factor in the nascent internal state content of each chemical species. The observed vibrational and rotational state distributions of the reaction products encode information about the structures of and relative fluxes through multiple TS regions, as well as the dynamics from the TS on to products. Acquisition of such information over a range of rotation–vibration quantum numbers is a nontrivial challenge that requires both high resolution and the ability to sample the populations of a wide range of quantum states* (6–28).

Chirped-pulse Fourier transform millimeter-wave (CPmmW) spectroscopy (29–38) is capable of recording, in each chirp, a several-gigahertz spectral region at submegahertz resolution. The chirped-pulse technique was developed (29–31) by Brooks Pate and coworkers at the University of Virginia for the microwave region and later extended to the millimeter-wave (mmwave) region by Field and coworkers (35), in collaboration with the Pate group and, independently, by Plusquellic and coworkers (34). Rotational spectroscopy is unsurpassed in its precision of sampling molecular geometric structure in the gas phase and its ability to resolve and vibrationally assign transitions, "vibrational satellites," that originate from different vibrational levels (39, 40). However, until the advent of CP techniques, it was only possible to exploit the high resolution and state specificity of microwave spectroscopy over sequential samples of few-megahertz spectral regions. Now, many new classes of rotational spectroscopy experiments are possible. For example, simultaneous broadband detection of isomerizing molecules enables "dynamic rotational spectroscopy" (31, 41). The relative transition intensities in CP experiments can be converted to branching ratios of multiple reaction products for chemical kinetics studies (42–45). A recent study of 193-nm photolysis of vinyl cyanide (VCN) in a room-temperature reactor revealed a new pathway to HCCCN by measuring the time evolution of the vibrational-level population distribution (VPD) in a CPmmW spectrum (43). Precise determination of (averaged) molecular structure remains at the core of these new directions, while broad spectral range and line intensities at ∼20% relative accuracy enable new chemical applications.

In this work, we utilize the VPD measured over several gigahertz of pure rotational CPmmW spectrum to sample the properties of TSs. We studied the 193-nm photolysis of VCN (acrylonitrile) in a supersonic jet and identified 2 distinct sets of VPDs of HCN reaction products. Both the structures of the TSs and the branching

Significance

Transition states control results of molecular reactions. However, it is difficult to extract details about the transition state solely from the chemical products born from the transition state. This inability to experimentally characterize transition state limits our ability to predict and steer the outcomes of chemical processes. Here we describe the use of a recently developed, simultaneously broadband and high-resolution technique, chirped-pulse millimeter-wave spectroscopy, to measure the nascent product state distribution that results from the photolysis of vinyl cyanide and, from it, to infer properties of the transition state(s) involved. Insights gleaned from studies such as these are crucial to a detailed understanding of molecular quantum dynamics at a level that promises to allow us to calculate and manipulate chemistry.

Author contributions: K.P., J.H.B., G.B.P., and R.W.F. designed research; K.P., J.H.B., P.B.C., R.G.S., J.S.M., S.J.K., and R.W.F. performed research; K.P. contributed new reagents/analytic tools; K.P., V.Y.C., J.H.B., P.B.C., S.J.K., and R.W.F. analyzed data; and K.P., J.H.B., S.J.K., and R.W.F. wrote the paper.

Reviewers: B.H.P., University of Virginia; and R.N.Z., Stanford University.

The authors declare no competing interest.

[1]To whom correspondence may be addressed. Email: rwfield@mit.edu.

This article contains supporting information online at https://www.pnas.org/lookup/suppl/doi:10.1073/pnas.1911326116/-/DCSupplemental.

First published December 18, 2019.

*H. A. Bechtel, A. H. Steeves, R. W. Field, Pure rotational spectroscopy as a probe of photodissociation dynamics in *61st International Symposium on Molecular Spectroscopy* (Columbus, OH, 2006), Presentation TH13.

between the corresponding product channels are extracted from the VPDs.

Photolysis of ethylene (13) and its substituted analogs, VCN (12, 22, 46–52), vinyl chloride (15, 23, 25, 26), vinyl bromide (17, 24, 53, 54), vinyl iodide (55), and propene (56), has been extensively studied during the last 4 decades. The 193-nm photolysis (57) of VCN has been observed (12, 22, 43, 47, 49) and calculated (43, 48, 50, 52) to take place via a dizzying array of reaction pathways. Since many of these pathways lead to difficult-to-distinguish final product channels, it has been challenging to obtain definitive experimental evidence in support of a particular model or theoretical description. We assume here that dissociation occurs on the ground electronic potential surface of VCN after rapid electronic relaxation and intramolecular redistribution of the photon energy (12, 58).

The present paper is primarily based on further analysis of measurements reported earlier (38), and the experimental details are available in *SI Appendix, Experimental Details*. and ref. 38. In particular, the spectrum of the VCN photolysis products, HCN and HNC, in the 86.5- to 93.0-GHz region is republished from ref. 38 in Fig. 1, now displaying assignments of multiple HCN and HNC $J = 1$–0 rotational transitions to various vibrational states of these isomers. The HCN and HNC transition frequencies are listed in *SI Appendix*, Table S1. In our previous work (38) we observed multiple HCN and HNC transitions that were attributed to the vibrationally excited molecules and assigned a few of them. We noticed (figure 15 of ref. 38) that deuteration to CH_2CDCN had a surprisingly modest effect on the observed total HCN vibrational population. We expected most of DCN to originate from the 3-center unimolecular elimination mechanism $CH_2CDCN \rightarrow CH_2C$: + DCN and to replace the majority of HCN upon deuteration of the precursor. In this work we examine the CPmmW spectrum of DCN and investigate its VPD in comparison with that of HCN.

Vibrational excitations cause small changes in rotational constants, and thus pure rotation transitions associated with different vibrational levels are easily resolved and assigned in the CPmmW spectrum. In HCN and HNC, the vibrational quantum numbers are (v_1, v_2, v_3), where v_1 designates the number of quanta in the C–H stretch of HCN and N–H stretch for HNC, v_2 in the bend, and v_3 in the C–N stretch. Since only $J = 1$–0 transitions fall within the present spectral range of our CPmmW spectrometer, transitions involving vibrational angular momentum $\ell > 0$ cannot be observed, and the corresponding quantum number label is omitted. This restriction to $\ell = 0$ renders all odd-v_2 vibrational levels of HCN and HNC unobservable with our spectrometer. The vibrational state assignment procedure is described in *SI Appendix*. Apropos of v_2 and ℓ, it is important to note that even $\Delta\ell$ relaxation within a given v_2 is expected to be fast, similar to rotational cooling; however, odd $\Delta\ell$ changes are necessarily vibrational ($\Delta v_2 \neq 0$) in nature, and therefore less efficient. The only $\ell = 0$ states with bending excitation are (0, 0, 0), (0, 2, 0), (0, 4, 0), and so on, and their combinations with stretching vibrations.

We begin by analyzing the dynamical information encoded in the frequencies of the rotational transitions. An isomerization reaction may be enabled by high vibrational excitation and large amplitude motion in the parent molecule (4, 31, 59–61). Because of the $I = 1$ nuclear spin of the ^{14}N atom and its electric quadrupole interaction with the electric field of the electrons in the molecule, the electric quadrupole constant $(eQq)_N$ is a sensitive diagnostic for HCN ↔ HNC isomerization dynamics. As the [H, C, N] molecule proceeds along the isomerization path via highly excited bending states, the evolution of the electronic configuration is probed by the strong vibrational-level dependence of the $(eQq)_N$ constant (59, 61, 62). Previously observed (38) rotational transitions of the HCN and HNC products of VCN photolysis are assigned here to vibrational levels up to $v_2 = 14$ in HCN and $v_2 = 8$ in HNC, and the corresponding $(eQq)_N$ constants are determined (see *SI Appendix* for details). Fig. 2 shows the dependence of the $(eQq)_N$ constant on the bending vibrational quantum on both sides of the HCN/HNC barrier and at vibrational energies up to 9,488.5 cm^{-1}, measured from the HCN (0,0,0) ground state.

Although the vibrational term energies of many HCN and HNC levels are separately known from Fourier transform infrared studies (63, 64) with a precision of 0.001 cm^{-1} or better, the energy of the HNC levels relative to those of HCN is much less well characterized. The experimental value (65) of 14.8 ± 2 kcal/mol

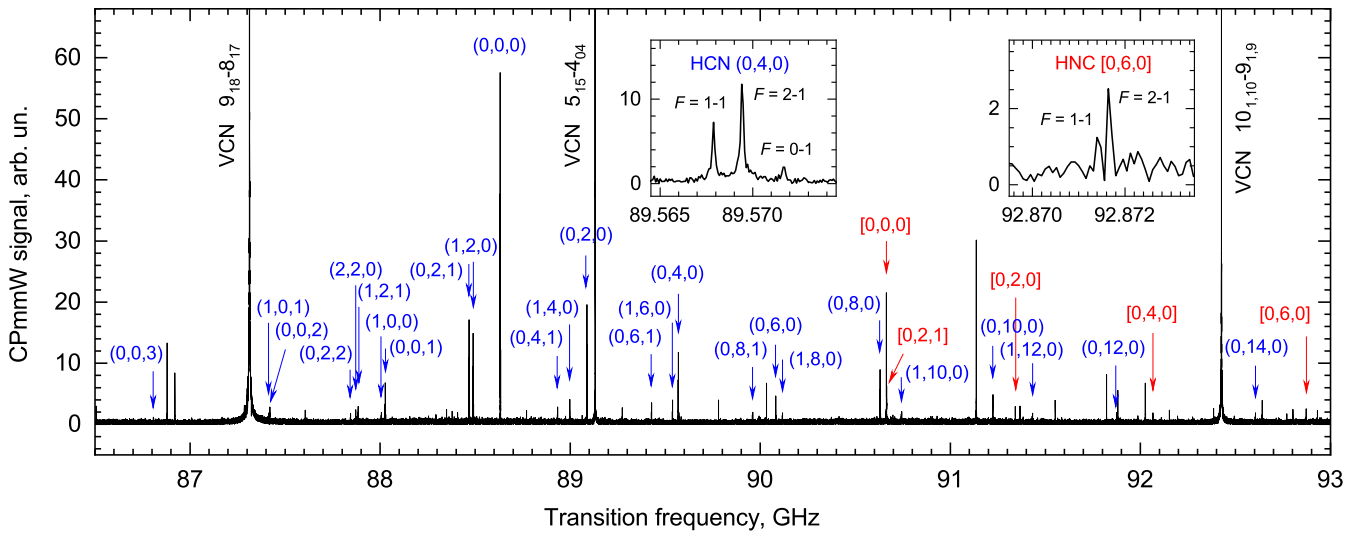

Fig. 1. CPmmW spectrum of the HCN and HNC photolysis products in the 86.5 to 93.0 GHz region with vibrationally assigned HCN and HNC rotational $J = 1$–0 transitions. The HCN and HNC transition frequencies are listed in *SI Appendix*, Table S1. The vibrational states (v_1 = C–H or N–H stretch, v_2 = bend, v_3 = C–N stretch) of HCN and HNC molecules are shown in round and square brackets, respectively, near their rotational lines. Two insets illustrate the electric quadrupole hyperfine $(eQq)_N$ structure, with the assignments. The chirp covers the 84.5- to 97.0-GHz region, but only the region containing the observed HCN and HNC transitions is shown. The spectrum and the FID are available in Datasets S1 and S2, respectively. The laser-off background spectrum and FID are given in Datasets S3 and S4, respectively. arb. un., arbitrary units. Adapted from ref. 38 with permission from The Royal Society of Chemistry.

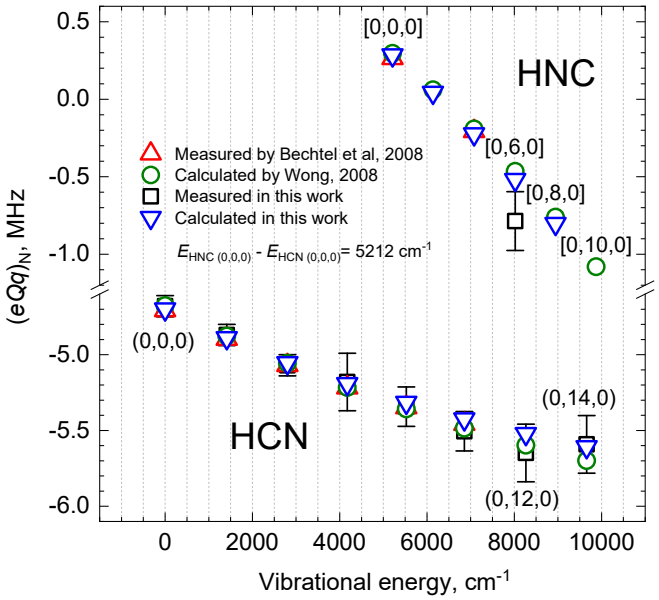

Fig. 2. Comparison of the $(eQq)_N$ constants between the previous calculations by Wong (61), previous experiment by Bechtel et al. (59), and the present work. The details of the calculations are available in *SI Appendix*. In order to position the ladder of HNC vibrational levels opposite to the ladder of HCN levels across the HCN ↔ HNC isomerization barrier, we use the $E_{HNC[0,0,0]} - E_{HCN(0,0,0)} = 5{,}212$ cm^{-1} value (68) for the energy difference between the 2 isomers. The HNC [0,6,0] $(eQq)_N$ value measured in this work deviates from the prediction (61) toward the HCN $(eQq)_N$ values and is in close resonance with the HCN (0,12,0) level. This may encode evidence of a resonant tunneling interaction between the HCN and HNC isomers.

(5,176 ± 700 cm^{-1}) is too uncertain to draw conclusions about the relative energies of the HCN and HNC vibrational levels. Recently, the combination of high-accuracy HEAT-456QP calculations and the Active Thermochemical Tables (ATcT) approach (66, 67) produced (68) a recommended value of 5,212 ± 30 cm^{-1} for the $E_{HNC[0,0,0]} - E_{HCN(0,0,0)}$ energy difference, which we adopt in this study. Thus, the plot in Fig. 2 puts the $(eQq)_N$ values of both isomers on a common energy scale.

The values of $(eQq)_N$ in HCN (0, v_2, 0) states decrease nearly linearly with v_2 and in agreement with the calculation (61) up to 14 quanta of bending excitation. Eventually, at $v_2 > 24$, the $(eQq)_N$ curve for HCN is predicted to converge with that for HNC (59). We observe that the calculated value of HNC [0,6,0] $(eQq)_N$ is outside the 1σ but within the 2σ experimental uncertainty of the measured value. The accepted value (68) of $E_{HNC[0,0,0]} - E_{HCN(0,0,0)} = 5{,}212$ cm^{-1} puts the HNC [0,6,0] level in near-resonance with the HCN (0,12,0) level across the isomerization barrier. Delocalization of the vibrational levels of the 2 isomers has been calculated (69, 70) for the near-transition-state energies of ∼15,000 cm^{-1} and above, which lies at significantly higher energy than the $E_{HCN(0,14,0)} = 9{,}488.5$ cm^{-1} and $E_{HNC[0,6,0]} \sim 8{,}021$ cm^{-1} energies that we reach in this work. In principle, accidental resonances are possible and those can lead to calculable mixing between HCN and HNC basis states at lower energies.

Because our current experiment is limited to $J = 1$–0 pure rotational transitions of H(D)CN, we cannot observe transitions between the states that possess nonzero vibrational angular momentum, ℓ. One might expect that the photodissociation of VCN is contained in the plane defined by the H, C, and N atoms, and therefore no HCN bending out of that plane would be allowed, and thus the vibrational angular momentum should be $\ell = 0$ for all HCN and HNC products. However, quasi-classical trajectory calculations suggest that HCN elimination is not constrained in a plane and predict the average value of the vibrational angular momentum $\langle\ell\rangle$ to be 2.8 and 2.5 for 3-center and 4-center mechanisms, respectively (52). For linear molecules, dynamics of the vibrational angular momentum defined by the TS properties and subsequent relaxation can affect the populations of rotational levels with specific symmetries. Future experimental observations of rotational transitions between $J > 0$ levels of HCN at higher mm-wave frequencies will reveal those ℓ-excitations.

We now turn to examination of the intensities of the spectral transitions, which encode important chemical information in addition to that obtained from transition frequencies. Specifically, the intensities of rotational transitions of molecules in vibrationally excited states are related to the VPD of those molecules, and a previously unobserved class of information about the 193-nm photolysis TS(s) of VCN is encoded in the VPDs of HCN and DCN.

Fitting the measured VPDs with a physically meaningful function can be a powerful tool in decoding the experimental data. Such VPDs depend on the vibrational wavefunctions of both the TS and photofragments and on the dynamics from the TS onward. Thus it seems appropriate to invoke generalized Franck–Condon overlap integrals of these vibrational wavefunctions for VPD analysis (71–73). Franck–Condon overlaps of vibronic levels have been extensively analyzed and applied to extract vibrational populations (74–82). Ruscic (81) has shown that the distribution of Franck–Condon overlap integrals in photoelectron spectra is well represented by the Poisson distribution if a harmonic potential approximation can be adopted. Klemperer and coworkers (82) have used Gaussian and Poisson functions to fit vibrationally resolved dispersed fluorescence spectra. The Poisson distribution had been invoked to describe the VPDs that result from electronic-to-vibrational collisional energy transfer (83, 84). On the other hand, theoretical (85–87) and experimental (21) work has been done to extend the Franck–Condon principle beyond electronic transitions and into the realm of reaction dynamics. Here we propose use of the generalized Franck–Condon principle to analyze the TS properties by fitting the experimental VPDs to a Poisson-type function:

$$P(n,\lambda) = A\frac{\lambda^n}{n!}, \qquad [1]$$

where $P(n)$ is the concentration of a product species with n vibrational quanta in a certain mode and A and λ are the adjustable parameters.

In an attempt to obtain more detailed information on the various channels leading to HCN products, we photodissociated

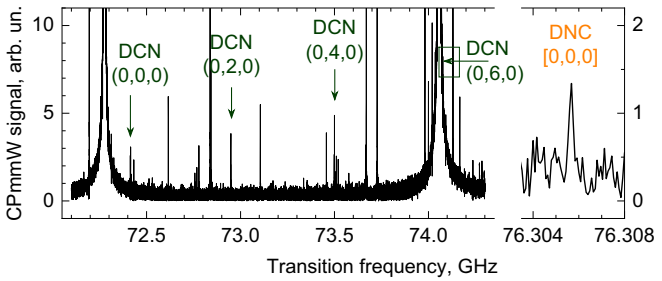

Fig. 3. CPmmW spectrum of the singly deuterated isotopologue of VCN, CH_2CDCN, and its DCN and DNC photofragments in several vibrational states. The 2 strong transitions of the parent CH_2CDCN molecule are $J_{KaKc} = 8_{18}$ to 7_{17} at 72.275 GHz and $J_{KaKc} = 8_{08}$ to 7_{07} at 74.057 GHz. The DCN (0,6,0) lines are situated on the shoulder of the CH_2CDCN line. The DNC spectrum was obtained with a narrow chirp centered at the line. arb. un., arbitrary units. The DCN and DNC transition frequencies are listed in *SI Appendix*, Table S2. The laser-on and laser-off spectra are available in Datasets S5 and S6, respectively.

deuterated VCN, CH_2CDCN. The corresponding spectra of HCN and DCN are shown in figure 15 of ref. 38 and in Fig. 3, respectively. In this test, we expected that unimolecular DCN elimination would proceed via the 3-center TS in which CN forms a bond with D, whereas the HCN would be formed by the 4-center unimolecular elimination TS. Most recent calculations predict dominance of the 3-center mechanism in HCN elimination from VCN over all other channels (43, 50, 52). As a consequence, in photolysis of a precursor that is singly deuterated near the cyano group, one would expect dominance of the DCN product accompanied by a 4-fold decrease in the HCN population. However, in figure 15 of ref. 38 we show that only an approximate 20% decrease in HCN signal is observed in our experiments as a result of deuteration of the VCN parent molecule. This suggests that DCN is formed with smaller branching ratio than HCN. In this work, we investigate the qualitative behavior of these HCN and DCN products' VPDs.

The VPDs of HCN and DCN, plotted as a function of bending mode population, are presented in Fig. 4, where 2 quanta of the HCN or DCN bend mode are the abscissa unit. The HCN VPD is from the line intensities published in figures 14 and 15 of ref. 38. We find that the DCN VPD can be well approximated by Eq. **1** with $\lambda = 2$ and also closely resembles the Vázquez and Martínez-Núñez results (52) of the trajectory calculations. The presumed 4-center TS-associated distribution of HCN vibrational population is better fit by an exponential rather than by a weighted Poisson distribution of Eq. **1** and qualitatively differs from the calculated (52) one. The observed non-Boltzmann DCN VPD shows that vibrational cooling does not erase the information encoded by TSs in the nascent vibrational state distributions.

The DCN VPD in Fig. 4 reaches a maximum at $v_2 = 4$ pure bending excitation, which is similar to the VPDs calculated for both the 3-center and newly discovered "CCdiss" elimination mechanisms (52). We therefore assign the DCN products to a combination of these 2 reaction pathways, with the 3-center pathway dominating. The exponentially decaying VPD of HCN in photodissociation of CH_2CDCN in Fig. 4 is maximum at $v_2 = 0$, suggesting that the geometry of H, C, and N atoms in that TS is near-linear. However, we cannot at this point relate that distribution and the associated TS properties to any HCN elimination mechanism that has been considered in the literature. The TS branching deduced from Fig. 4 is DCN: HCN = 1: 4, which is consistent with the previously observed depletion of the HCN signal upon deuteration of the precursor. Thus, while the 3-center mechanism is expected to be the dominant pathway to HCN, according to our results it accounts for only 20% of H(D)CN. The 80% majority of the H(D)CN observed in this work is associated with a presently unidentified reaction mechanism.

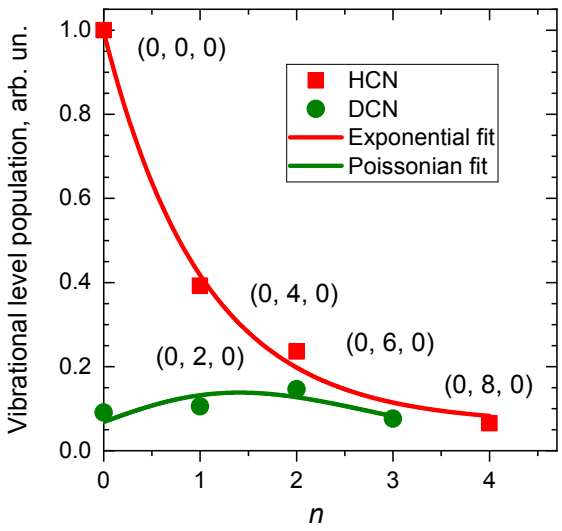

Fig. 4. Poisson and exponential fits of the HCN and DCN data. The rotational line intensities of pure bending vibrational levels of the HCN and DCN product molecules that result from CH_2CDCN 193 nm photolysis are integrated over their hyperfine components and corrected for the frequency-dependent transmission curve of the CPmmW spectrometer. The relative intensities of the excitation chirp between the 68.7 ← 78.7 GHz and 84.4 → 97.0 GHz chirping regions for DCN, DNC, and HCN, HNC were independently verified to be comparable by referencing them to a $T_{rot} = 6 \pm 1$ K PGOPHER (92) simulation of the parent CH_2CDCN transitions. No adjustment of intensities for the chirp direction (34) was made since the spectral regions of interest are significantly smaller than the chirp ranges (93). Data for the HCN plot from ref. 38. arb. un., arbitrary units.

The estimated several possible ways in which the chemically unassigned part of the HCN VPD could stem from bimolecular reaction pathways in the collisional region of the slit jet expansion. The details are given in *SI Appendix*. We estimate that the branching ratio for a $CH_2CCN + CH_2CHCN \rightarrow C_5H_4N + HCN$ channel relative to that for the 3-center HCN elimination is $<4 \times 10^{-3}$ and thus exclude this possibility. For the $CH_2CCN + CH_2CCN \rightarrow C_5H_3N + HCN$ reaction the same branching ratio is estimated to be $<3 \times 10^{-2}$. In that radical–radical self-reaction, the HCN photofragments are expected to be highly energized rotationally, and unlikely to be detectable. We evaluate the upper bound for the CN radical elimination channel $CH_2CHCN \rightarrow CH_2CH + CN$ branching to be 0.01 relative to the 3-center HCN channel. Although H-atom abstraction by CN is barrierless, the concomitant energy release will reduce the observable CPmmW signal unless perfect rotational cooling of HCN is achieved in the jet.

Finally, we consider a free H-atom attacking a CH_2CHCN molecule and eliminating HCN: $H + CH_2CHCN \rightarrow CH_2CH + HCN$. Using the ATcT results from the SI appendix, table S5 of ref. 43, we find that this reaction is slightly endothermic: $\Delta_r H°(0K) = 5.01$ kcal/mol. According to the photofragment translational spectroscopy study of Hall and coworkers (12), the average kinetic energy release in the $CH_2CHCN \rightarrow CH_2CCN + H$ reaction is near 4 kcal/mol, with its distribution extending to 10 kcal/mol. Most of it will be deposited in the kinetic energy of the light H-atom, which might then be able to surmount (or tunnel through) the barrier of 7.1 kcal/mol for its addition to CH_2CHCN. Decomposition of the adduct may potentially lead to colder HCN products. This decomposition has a relatively high barrier of 10.5 kcal/mol relative to the initial reactants but may still occur via tunneling. Note that these barriers are obtained here by CCSD(T)/CBS//CCSD(T)/cc-pVTZ calculations. We leave more detailed theoretical and experimental exploration of this possibility for future studies.

A fundamental difficulty in the use of CPmmW spectroscopy is understanding how the observed intensity of only one rotational transition relates to a vibrational population. The relevant equations require the existence and knowledge of the rotational temperature (43). The contribution to our measured VPD from TSs that release products with very high rotational excitation (23, 24, 26, 54), which are not thermalized to the ambient temperature in the detection volume, will be underestimated relative to nascent product populations in the low-J states (43). Even if more than one rotational transition for each vibrational level can be measured, the nascent rotational-level population distribution (RPD) may not be Boltzmann, in which case the rotational temperature that is needed for intensity calibration is undefined.

The RPD affects these CPmmW measurements of relative vibrational level populations in several ways. 1) It is necessary to assume that in the supersonic expansion rotational relaxation is much faster than vibrational relaxation; 2) rotational populations in every vibrational level are thermalized; 3) the rotational temperature in every vibrational level is the same; 4) the rotational temperature of the photofragment molecules (HCN, HNC) is the same as that of the parent molecule (VCN), which acts as a

thermometer; and 5) there is no significant population in very-high-J, rotational levels which are too highly excited to be thermalized in the supersonic expansion.

Here we assume that the RPD in the mm-wave interaction region is the same for every vibrational level of a product molecule. That assumption relies on the effectiveness and uniformity of postphotolysis rotational cooling in the quasi-1-dimensional expansion from the slit-shaped nozzle (88), and on the trajectory calculations (52) of nascent HCN RPDs that predict similar rotational temperatures for HCN eliminated via 3-center, 4-center, and the newly discovered CCdiss mechanisms: 6725 K, 5372 K, and 3133 K, respectively. We also assume that for small linear molecules with sparse vibrational levels, like HCN, vibrational energy redistribution is slow (42, 89) compared to rotational cooling and the VPDs are not significantly altered. The highly nonthermal DCN VPD suggests that in this experiment vibrational cooling is incomplete and less effective than rotational cooling. If these assumptions are valid, which we presently have no independent way to confirm, then, for each product molecule formed via any TS the relative intensities in Fig. 4 would represent the nascent VPDs (23, 24, 26, 43, 52, 54). Hence, the origin of the strong HCN signal with an exponential VPD eludes definitive explanation. Although we considered various bimolecular possibilities for alternative sources of cold HCN, our calculations and estimations identified no plausible candidates, with the possible exception of translationally hot H-atoms reacting with VCN.

In summary, we have used CPmmW spectroscopy to investigate previously unknown chemical pathways to HCN following 193-nm photodissociation of VCN. The toolbox consists of measuring the vibrational population distribution of photolysis products and isotopic labeling of the precursor molecule: CH_2CDCN. The broadband and high-resolution features of CPmmW spectroscopy enable us to observe the HCN, HNC, DCN, and DNC products and their vibrational population distributions. The relative intensities of the CPmmW rotational transitions reveal the functional dependences of vibrational-mode populations in these products. A Poisson-like DCN VPD is consistent with the combination of the 3-center and CCdiss reaction channels in unimolecular photodissociation of CH_2CDCN. The exponential HCN VPD points to the existence of an unexpected reaction pathway likely outside of known unimolecular dissociation channels in VCN. The experimental evidence for this previously unknown reaction channel has directed us to consider bimolecular chemistry in the supersonic expansion. Our calculations suggest that a possible route is the H-atom addition/HCN elimination reaction H + $CH_2CHCN \rightarrow CH_2CH + HCN$. This work demonstrates that the CPmmW technique has promise for characterization of TSs of chemical reactions. The ability to sample additional (higher-J) rotational transitions to better characterize the rotational temperatures of the photolysis products and the use of additional parent molecule isotopologues are desirable next steps, especially when complemented by rotationally and vibrationally level-resolved calculations of product yields.

Experimental Methods

The CPmmW spectrometer employs an 8-GS/s arbitrary waveform generator to create chirped pulses and a 50-GS/s, 12.5-GHz bandwidth oscilloscope to digitize the free induction decay (FID) (35). Two active multiplier chains were used to reach the mm-wave regions of 68.7 to 78.7 GHz and 84.4 to 97.0 GHz by frequency multiplication. A phase-locked Gunn oscillator provides a single frequency for heterodyne detection of the FID. The VCN molecules entrained in argon carrier gas at 0.25% by mole at a total stagnation pressure of 150 mbar were expanded into a 5×10^{-4}-mbar vacuum from a pulsed slit-shaped nozzle (88, 90, 91) and photolyzed by an unfocused 1-cm × 2.5-cm 193-nm laser beam 1.5 cm downstream along the expansion path (38). The laser beam propagates in the direction that is perpendicular to both the slit and the molecular beam expansion direction. The 2.5-cm side of the rectangular cross-section of the laser beam is parallel to the slit. The slit opening is 5 cm long and 0.02 cm wide.

Data Availability

The detailed description of the experiment, spectroscopic and kinetic considerations, line lists of HCN, HNC, DCN, and DNC rotational transitions with their vibrational level assignments, calculated $(eQq)_N$ constants, and description of the theoretical methods used in this work are available in *SI Appendix*. The links to the computational codes are available in the references section of *SI Appendix*. The averaged FIDs and the CPmmW spectra are given in Datasets S1–S6 as described in the figure legends.

ACKNOWLEDGMENTS. We thank Dr. Georg Mellau for his advice on the assignments of the $v_2 = 12$ and 14 vibrational levels of HCN. K.P. thanks Branko Ruscic for helpful discussions. We thank the Department of Energy (grant DEFG0287ER13671) for providing primary support of this work (equipment and personnel support for R.G.S.), the Petroleum Research Fund (grant 50650-ND6) for support of K.P., and the National Science Foundation (grant 1126380) for equipment support. K.P. and S.J.K. acknowledge the support by the US Department of Energy, Office of Science, Office of Basic Energy Sciences, Division of Chemical Sciences, Geosciences, and Biosciences under contract DE-AC02-06CH11357. V.Y.C. was supported by the US Department of Energy, Office of Science, Basic Energy Sciences, Materials Sciences and Engineering Division, Condensed Matter Theory Program.

1. P. G. Wenthold, D. A. Hrovat, W. T. Borden, W. C. Lineberger, Transition-state spectroscopy of cyclooctatetraene. *Science* **272**, 1456–1459 (1996).
2. W. H. Green, C. B. Moore, W. F. Polik, Transition states and rate constants for unimolecular reactions. *Annu. Rev. Phys. Chem.* **43**, 591–626 (1992).
3. C. Wittig, I. Bezel, Effective Hamiltonian models and unimolecular decomposition. *J. Phys. Chem. B* **110**, 19850–19860 (2006).
4. J. H. Baraban *et al*., Spectroscopic characterization of isomerization transition states. *Science* **350**, 1338–1342 (2015).
5. J. C. Polanyi, A. H. Zewail, Direct observation of the transition state. *Acc. Chem. Res.* **28**, 119–132 (1995).
6. G. L. Barnes, W. L. Hase, Transition state analysis: Bent out of shape. *Nat. Chem.* **1**, 103–104 (2009).
7. E. R. Lovejoy, S. K. Kim, C. B. Moore, Observation of transition-state vibrational thresholds in the rate of dissociation of ketene. *Science* **256**, 1541–1544 (1992).
8. P. L. Houston, C. B. Moore, Formaldehyde photochemistry: Appearance rate, vibrational relaxation, and energy distribution of the CO product. *J. Chem. Phys.* **65**, 757–770 (1976).
9. F. F. Crim, Vibrationally mediated photodissociation: Exploring excited-state surfaces and controlling decomposition pathways. *Annu. Rev. Phys. Chem.* **44**, 397–428 (1993).
10. W. R. Simpson, T. P. Rakitzis, S. A. Kandel, T. Lev-On, R. N. Zare, Picturing the transition-state region and understanding vibrational enhancement for the $Cl + CH_4 \rightarrow HCl + CH_3$ reaction. *J. Phys. Chem.* **100**, 7938–7947 (1996).
11. S. W. North, G. E. Hall, Vector and scalar correlations in statistical dissociation: The photodissociation of NCCN at 193 nm. *J. Chem. Phys.* **106**, 60–76 (1997).
12. D. A. Blank, A. G. Suits, Y. T. Lee, S. W. North, G. E. Hall, Photodissociation of acrylonitrile at 193 nm: A photofragment translational spectroscopy study using synchrotron radiation for product photoionization. *J. Chem. Phys.* **108**, 5784–5794 (1998).
13. B. A. Balko, J. Zhang, Y. T. Lee, Photodissociation of ethylene at 193 nm. *J. Chem. Phys.* **97**, 935–942 (1992).
14. S. A. Lahankar *et al*., The roaming atom pathway in formaldehyde decomposition. *J. Chem. Phys.* **125**, 44303 (2006).
15. R. Fernando, C. Qu, J. M. Bowman, R. W. Field, A. G. Suits, Does infrared multiphoton dissociation of vinyl chloride yield cold vinylidene? *J. Phys. Chem. Lett.* **6**, 2457–2462 (2015).
16. M. Ryazanov, C. Rodrigo, H. Reisler, Overtone-induced dissociation and isomerization dynamics of the hydroxymethyl radical (CH_2OH and CD_2OH). II. Velocity map imaging studies. *J. Chem. Phys.* **136**, 084305 (2012).
17. D. K. Liu, L. T. Letendre, H. L. Dai, 193 nm photolysis of vinyl bromide: Nascent product distribution of the $C_2H_3Br \rightarrow C_2H_2$ (vinylidene) plus HBr channel. *J. Chem. Phys.* **115**, 1734–1741 (2001).
18. D. P. Baldwin, M. A. Buntine, D. W. Chandler, Photodissociation of acetylene: Determination of D_0^0(HCC–H) by photofragment imaging. *J. Chem. Phys.* **93**, 6578–6584 (1990).
19. A. H. Steeves, A. J. Merer, H. A. Bechtel, A. R. Beck, R. W. Field, Direct observation of the symmetric stretching modes of $\tilde{A}\ ^1A_u$ acetylene by pulsed supersonic jet laser induced fluorescence. *Mol. Phys.* **106**, 1867–1877 (2008).
20. D. H. Mordaunt *et al*., Near threshold photodissociation of acetylene. *J. Chem. Phys.* **108**, 519–526 (1998).
21. J. Zhang *et al*., State to state to state dynamics of the $D + H_2 \rightarrow HD + H$ reaction: Control of transition-state pathways via reagent orientation. *Phys. Rev. Lett.* **96**, 093201 (2006).
22. M. J. Wilhelm, M. Nikow, L. Letendre, H. L. Dai, Photodissociation of vinyl cyanide at 193 nm: Nascent product distributions of the molecular elimination channels. *J. Chem. Phys.* **130**, 044307 (2009).
23. S. R. Lin *et al*., I. Three-center versus four-center HCl-elimination in photolysis of vinyl chloride at 193 nm: Bimodal rotational distribution of HCl ($v \leq 7$) detected with time-resolved Fourier-transform spectroscopy. *J. Chem. Phys.* **114**, 160–168 (2001).

24. S. R. Lin *et al*., Three-center versus four-center elimination in photolysis of vinyl fluoride and vinyl bromide at 193 nm: Bimodal rotational distribution of HF and HBr ($v \leq 5$) detected with time-resolved Fourier transform spectroscopy. *J. Chem. Phys.* **114**, 7396–7406 (2001).
25. M. Umemoto *et al*., Photofragmentation of mono- and dichloroethylenes: Translational energy measurements of recoiling Cl and HCl fragments. *J. Chem. Phys.* **83**, 1657–1666 (1985).
26. Y. B. Huang, Y. A. Yang, G. X. He, R. J. Gordon, The ultraviolet photodissociation dynamics of d_1-vinyl chloride. *J. Chem. Phys.* **99**, 2752–2759 (1993).
27. W. W. Harper, S. A. Nizkorodov, D. J. Nesbitt, Reactive scattering of F + HD → HF(*v, J*) + D: HF(*v, J*) nascent product state distributions and evidence for quantum transition state resonances. *J. Chem. Phys.* **116**, 5622–5632 (2002).
28. J. H. Lehman *et al*., Collisional quenching of OD A $^2\Sigma^+$ by H_2: Experimental and theoretical studies of the state-resolved OD X $^2\Pi$ product distribution and branching fraction. *J. Chem. Phys.* **133**, 164307 (2010).
29. G. G. Brown, B. C. Dian, K. O. Douglass, S. M. Geyer, B. H. Pate, The rotational spectrum of epifluorohydrin measured by chirped-pulse Fourier transform microwave spectroscopy. *J. Mol. Spectrosc.* **238**, 200–212 (2006).
30. G. G. Brown *et al*., A broadband Fourier transform microwave spectrometer based on chirped pulse excitation. *Rev. Sci. Instrum.* **79**, 053103 (2008).
31. B. C. Dian *et al*., Conformational isomerization kinetics of pent-1-en-4-yne with 3,330 cm^{-1} of internal energy measured by dynamic rotational spectroscopy. *Proc. Natl. Acad. Sci. U.S.A.* **105**, 12696–12700 (2008).
32. B. C. Dian, G. G. Brown, K. O. Douglass, B. H. Pate, Measuring picosecond isomerization kinetics via broadband microwave spectroscopy. *Science* **320**, 924–928 (2008).
33. B. H. Pate, F. C. De Lucia, Broadband molecular rotational spectroscopy special issue. *J. Mol. Spectrosc.* **280**, 1–2 (2012).
34. E. Gerecht, K. O. Douglass, D. F. Plusquellic, Chirped-pulse terahertz spectroscopy for broadband trace gas sensing. *Opt. Express* **19**, 8973–8984 (2011).
35. G. B. Park, A. H. Steeves, K. Kuyanov-Prozument, J. L. Neill, R. W. Field, Design and evaluation of a pulsed-jet chirped-pulse millimeter-wave spectrometer for the 70-102 GHz region. *J. Chem. Phys.* **135**, 024202 (2011).
36. M. Schnell, Broadband rotational spectroscopy for molecular structure and dynamics studies. *Z. Phys. Chem.* **227**, 1–21 (2013).
37. G. B. Park, R. W. Field, Perspective: The first ten years of broadband chirped pulse Fourier transform microwave spectroscopy. *J. Chem. Phys.* **144**, 200901 (2016).
38. K. Prozument *et al*., A new approach toward transition state spectroscopy. *Faraday Discuss.* **163**, 33–57, discussion 117–138 (2013).
39. C. H. Townes, A. L. Schawlow, *Microwave Spectroscopy* (McGraw-Hill Book Company, New York, 1955).
40. E. B. Wilson, Jr, Microwave spectroscopy in chemistry. *Science* **162**, 59–66 (1968).
41. J. Keske, D. A. McWhorter, B. H. Pate, Molecular rotation in the presence of intramolecular vibrational energy redistribution. *Int. Rev. Phys. Chem.* **19**, 363–407 (2000).
42. K. Prozument *et al*., Chirped-pulse millimeter-wave spectroscopy for dynamics and kinetics studies of pyrolysis reactions. *Phys. Chem. Chem. Phys.* **16**, 15739–15751 (2014).
43. D. P. Zaleski, L. B. Harding, S. J. Klippenstein, B. Ruscic, K. Prozument, Time-resolved kinetic chirped-pulse rotational spectroscopy in a room-temperature flow reactor. *J. Phys. Chem. Lett.* **8**, 6180–6188 (2017).
44. B. M. Broderick, N. Suas-David, N. Dias, A. G. Suits, Isomer-specific detection in the UV photodissociation of the propargyl radical by chirped-pulse mm-wave spectroscopy in a pulsed quasi-uniform flow. *Phys. Chem. Chem. Phys.* **20**, 5517–5529 (2018).
45. J. P. Porterfield, S. Eibenberger, D. Patterson, M. C. McCarthy, The ozonolysis of isoprene in a cryogenic buffer gas cell by high resolution microwave spectroscopy. *Phys. Chem. Chem. Phys.* **20**, 16828–16834 (2018).
46. A. Gandini, P. A. Hackett, The photochemistry of acrylonitrile vapour at 213.9 nm. *Can. J. Chem.* **56**, 2096–2098 (1978).
47. A. Fahr, A. H. Laufer, The 1,1-elimination of HCN and formation of triplet vinylidene from the photolysis of acrylonitrile. *J. Phys. Chem.* **96**, 4217–4219 (1992).
48. A. Derecskei-Kovacs, S. W. North, The unimolecular dissociation of vinylcyanide: A theoretical investigation of a complex multichannel reaction. *J. Chem. Phys.* **110**, 2862–2871 (1999).
49. L. Letendre, H. L. Dai, Structure and vibrational modes of the cyanovinyl radical: A study by time-resolved fourier transform IR emission spectroscopy. *J. Phys. Chem. A* **106**, 12035–12040 (2002).
50. Z. Homayoon, S. A. Vázquez, R. Rodríguez-Fernández, E. Martínez-Núñez, Ab Initio and RRKM Study of the HCN/HNC Elimination Channels from Vinyl Cyanide, Ab initio and RRKM study of the HCN/HNC elimination channels from vinyl cyanide. *J. Phys. Chem. A* **115**, 979–985 (2011).
51. Z. Kisiel *et al*., Broadband rotational spectroscopy of acrylonitrile: Vibrational energies from perturbations. *J. Mol. Spectrosc.* **280**, 134–144 (2012).
52. S. A. Vázquez, E. Martínez-Núñez, HCN elimination from vinyl cyanide: Product energy partitioning, the role of hydrogen-deuterium exchange reactions and a new pathway. *Phys. Chem. Chem. Phys.* **17**, 6948–6955 (2015).
53. S. A. Abrash, R. W. Zehner, G. J. Mains, L. M. Raff, Theoretical-studies of the thermal gas-phase decomposition of vinyl bromide on the ground-state potential-energy surface. *J. Phys. Chem.* **99**, 2959–2977 (1995).
54. E. Martinez-Nunez, S. Vazquez, Rotational distributions of HBr in the photodissociation of vinyl bromide at 193 nm: An investigation by direct quasiclassical trajectory calculations. *Chem. Phys. Lett.* **425**, 22–27 (2006).
55. P. Zou *et al*., Ultraviolet photodissociation of vinyl iodide: Understanding the halogen dependence of photodissociation mechanisms in vinyl halides. *Phys. Chem. Chem. Phys.* **10**, 713–728 (2008).
56. Y. L. Zhao, A. H. Laufer, J. B. Halpern, A. Fahr, Hydrogen migration and vinylidene pathway for formation of methane in the 193 nm photodissociation of propene: $CH_3CH{=}CH_2$ and $CD_3CD{=}CD_2$. *J. Phys. Chem. A* **111**, 8330–8335 (2007).
57. P. A. Mullen, M. K. Orloff, The electronic spectrum of acrylonitrile. *Theor. Chim. Acta* **23**, 278–284 (1971).
58. W. N. Du, C. Luo, Z. S. Li, The photodissociation mechanisms of acrylonitrile: Ab initio calculations on reaction channels and surface intersections. *J. Chem. Phys.* **129**, 174309 (2008).
59. H. A. Bechtel, A. H. Steeves, B. M. Wong, R. W. Field, Evolution of chemical bonding during HCN ⇆ HNC isomerization as revealed through nuclear quadrupole hyperfine structure. *Angew. Chem. Int. Ed. Engl.* **47**, 2969–2972 (2008).
60. A. R. Sharma, J. M. Bowman, D. J. Nesbitt, Large-amplitude dynamics in vinyl radical: The role of quantum tunneling as an isomerization mechanism. *J. Chem. Phys.* **136**, 034305 (2012).
61. B. M. Wong, Nuclear quadrupole hyperfine structure in $HC^{14}N/H^{14}NC$ and $DC^{15}N/D^{15}NC$ isomerization: A diagnostic tool for characterizing vibrational localization. *Phys. Chem. Chem. Phys.* **10**, 5599–5606 (2008).
62. H. A. Bechtel, A. H. Steeves, R. W. Field, Laboratory measurements of the hyperfine structure of $H^{14}N^{12}C$ and $D^{14}N^{12}C$. *Astrophys. J.* **649**, L53–L56 (2006).
63. G. Ch. Mellau, Complete experimental rovibrational eigenenergies of HCN up to 6880 cm^{-1} above the ground state. *J. Chem. Phys.* **134**, 234303 (2011).
64. R. J. Barber *et al*., ExoMol line lists – III. An improved hot rotation-vibration line list for HCN and HNC. *Mon. Not. R. Astron. Soc.* **437**, 1828–1835 (2014).
65. C. F. Pau, W. J. Hehre, Heat of formation of hydrogen isocyanide by ion-cyclotron double-resonance spectroscopy. *J. Phys. Chem.* **86**, 321–322 (1982).
66. B. Ruscic *et al*., Introduction to active thermochemical tables: Several "key" enthalpies of formation revisited. *J. Phys. Chem. A* **108**, 9979–9997 (2004).
67. B. Ruscic *et al*., Active thermochemical tables: Thermochemistry for the 21st century. *J. Phys. Conf. Ser.* **16**, 561–570 (2005).
68. T. L. Nguyen, J. H. Baraban, B. Ruscic, J. F. Stanton, On the HCN - HNC energy difference. *J. Phys. Chem. A* **119**, 10929–10934 (2015).
69. J. M. Bowman, S. Irle, K. Morokuma, A. Wodtke, Dipole moments of highly vibrationally excited HCN: Theoretical prediction of an experimental diagnostic for delocalized states. *J. Chem. Phys.* **114**, 7923–7934 (2001).
70. T. Barger, A. M. Wodtke, J. M. Bowman, Radiative relaxation and isomeric branching of highly excited H/C/N: The importance of delocalized vibrational states. *Astrophys. J.* **587**, 841–846 (2003).
71. M. J. Berry, Golden rule calculation of reaction-product vibronic state distributions. *Chem. Phys. Lett.* **27**, 73–77 (1974).
72. M. Baer, Isotopic reactive systems H + Cl_2 and D + Cl_2. A quantum mechanical treatment of collinear arrangement. *J. Chem. Phys.* **60**, 1057–1064 (1974).
73. G. C. Schatz, J. Ross, Franck–Condon factors in studies of dynamics of chemical reactions. I. General theory, application to collinear atom–Diatom reactions. *J. Chem. Phys.* **66**, 1021–1036 (1977).
74. J. Tellinghuisen, Intensity factors for the I_2 $B \leftrightarrow X$ band system. *J. Quant. Spectrosc. Radiat. Transf.* **19**, 149–161 (1978).
75. J. R. Reimers, K. R. Wilson, E. J. Heller, Complex time dependent wave packet technique for thermal equilibrium systems: Electronic spectra. *J. Chem. Phys.* **79**, 4749–4757 (1983).
76. B. Ruscic, J. Berkowitz, Photoionization mass spectrometry of CH_2S and HCS. *J. Chem. Phys.* **98**, 2568–2579 (1993).
77. L. S. Cederbaum, W. Domcke, A many-body approach to vibrational structure in molecular electronic spectra. I. Theory. *J. Chem. Phys.* **64**, 603–611 (1976).
78. J. J. Valentini, J. B. Cross, The photodissociation cage effect in van der Waals complexes: Fluorescence spectra of I_2 B($^3\Pi_{0+u}$) from the hindered photodissociation of I_2Ar at 488 nm. *J. Chem. Phys.* **77**, 572–573 (1982).
79. D. Dehareng *et al*., Intramolecular dynamics by photoelectron spectroscopy. II. Nonadiabatic processes. *J. Chem. Phys.* **79**, 3719–3724 (1983).
80. J. M. Philippoz, H. van den Bergh, R. Monot, Product vibrational state distributions in the photodissociation of iodine–rare gas clusters. *J. Phys. Chem.* **91**, 2545–2550 (1987).
81. B. Ruscic, Fourier transform photoelectron spectroscopy: The correlation function and the harmonic oscillator approximation. *J. Chem. Phys.* **85**, 3776–3784 (1986).
82. A. E. Stevens Miller, C. C. Chuang, H. C. Fu, K. J. Higgins, W. Klemperer, Dynamics of linear and T-shaped Ar-I_2 dissociation upon $B \leftarrow X$ optical excitation: A dispersed fluorescence study of the linear isomer. *J. Chem. Phys.* **111**, 7844–7856 (1999).
83. R. D. Levine, R. B. Bernstein, Dynamical theory of vibrational state population distribution in electronic-to-vibrational energy transfer. Application to Hg*-sensitized IR fluorescence of diatomics. *Chem. Phys. Lett.* **15**, 1–6 (1972).
84. Y. Fushiki, S. Tsuchiya, Electronic-to-vibrational energy transfer in a collision of CO with Hg($^3P_0$). *Chem. Phys. Lett.* **22**, 47–51 (1973).
85. K. Schulten, R. G. Gordon, Quantum theory of angular momentum coupling in reactive collisions. *J. Chem. Phys.* **64**, 2918–2938 (1976).
86. G. C. Schatz, J. Ross, Franck–Condon factors in studies of dynamics of chemical reactions. II. Vibration–Rotation distributions in atom–diatom reactions. *J. Chem. Phys.* **66**, 1037–1053 (1977).
87. M. Gustafsson, R. T. Skodje, The state-to-state-to-state model for direct chemical reactions: Application to D + H_2 → HD + H. *J. Chem. Phys.* **124**, 144311 (2006).
88. K. Liu *et al*., A long path length pulsed slit valve appropriate for high temperature operation: Infrared spectroscopy of jet-cooled large water clusters and nucleotide bases. *Rev. Sci. Instrum.* **67**, 410–416 (1996).
89. R. L. Deleon, J. S. Muenter, Vibrational relaxation of linear molecules in a nozzle expansion. *Chem. Phys. Lett.* **111**, 147–150 (1984).
90. S. Wu, P. Dupré, T. A. Miller, High-resolution IR cavity ring-down spectroscopy of jet-cooled free radicals and other species. *Phys. Chem. Chem. Phys.* **8**, 1682–1689 (2006).
91. O. F. Hagena, Nucleation and growth of clusters in expanding nozzle flows. *Surf. Sci.* **106**, 101–116 (1981).
92. C. M. Western, PGOPHER: A program for simulating rotational, vibrational and electronic spectra. *J. Quant. Spectrosc. Radiat. Transf.* **186**, 221–242 (2017).
93. G. B. Park, R. W. Field, Edge effects in chirped-pulse Fourier transform microwave spectra. *J. Mol. Spectrosc.* **312**, 54–57 (2015).